Electron trapping in strong-field dissociative frustrated ionization of CO molecules

Wenbin Zhang,[1] Peifen Lu,[1] Xiaochun Gong,[1] Hui Li,[1] Qinying Ji,[1] Kang Lin,[1] Junyang Ma,[1] Hanxiao Li,[1] Fenghao Sun,[1] Junjie Qiang,[1] Fei Chen,[1] Jihong Tong,[1] and Jian Wu[1,2,*]

[1]*State Key Laboratory of Precision Spectroscopy, East China Normal University, Shanghai 200062, China*

[2]*Collaborative Innovation Center of Extreme Optics, Shanxi University, Taiyuan, Shanxi 030006, China*

(Received 27 November 2019; accepted 11 February 2020; published 3 March 2020)

We experimentally investigate the laser-induced dissociative frustrated multiple ionization of CO molecules; in this process one of the released electrons does not escape to the continuum but is eventually trapped into high-lying Rydberg states of the outgoing positively charged nuclear fragments at the ends of the laser pulse, leading to the formation of neutral Rydberg fragments, i.e., C^* or O^*. By measuring the ejected neutral Rydberg and ionic nuclear fragments as well as the freed electrons in coincidence, we trace the probability of electron trapping by different nuclear fragments and find that formation of C^* is preferred to O^*. Furthermore, the electron trapping to one of the outgoing nuclear fragments of the breaking molecule can be steered by using a phase-controlled two-color laser pulse. Our results show that Rydberg fragments are more likely to be produced for CO molecules when they are exposed to a laser field pointing from C to O. This orientation-dependent asymmetric emission of the neutral Rydberg fragments is further confirmed in the multiple ionization of CO molecules by using a single-color elliptically polarized femtosecond laser pulse.

DOI: 10.1103/PhysRevA.101.033401

I. INTRODUCTION

The ionization of atoms or molecules and the subsequent motion of the liberated electrons driven by a strong laser field give rise to a multitude of intriguing phenomena, such as above-threshold ionization [1,2], nonsequential double ionization [3,4], electron self-diffraction [5–7], and high-harmonic generation [8,9]. Rather than eventually escaping to the continuum, it was demonstrated that a substantial fraction of the liberated electrons can be trapped into high-lying Rydberg states at the ends of the strong laser pulse, leading to the formation of neutral Rydberg atoms [10–12]. In general, the underlying dynamics of the electron trapping can be understood by either the multiphoton resonant excitation [13–16] or frustrated tunneling ionization [17–19] depending on the laser wavelength and intensity. The electron-trapping-induced Rydberg excitation has attracted extensive attention in the past few years for accelerating and decelerating neutral particles [20,21], understanding the near-threshold harmonic generation [22] and the low-energy photoelectron spectral features [23], revealing multiphoton Rabi oscillation [24], and generating coherent extreme-ultraviolet light emission [25].

For multiple ionization of molecules, the liberated electrons can be trapped to the outgoing nuclear fragments, dubbed as the dissociative frustrated ionization (DFI) of molecules [26,27], which has been observed for various molecular systems such as H_2 [15,26,28], D_2 [29,30], O_2 [16], N_2 [31], D_3^+ [32], and clusters [33–36]. However, to our knowledge, as compared to the extensively investigated homonuclear molecules, experimental studies on the electron trapping dynamics in strong-field multiple ionization of heteronuclear molecules are rare in which the liberated electrons need to decide on which ionic fragments to be trapped to form different Rydberg atoms.

The CO molecule has been used as a prototype to reveal the strong-field dissociative ionization dynamics of heteronuclear molecules [37–42]. In this paper, we experimentally investigate the electron trapping in forming the Rydberg fragments of C^* or O^* in the DFI of CO molecules driven by femtosecond laser pulses. The coincidence measurements of the neutral Rydberg and charged particles ejected from the breaking molecules allow us to clearly identify different fragmentation channels. Our results show that the liberated electron is preferred to be trapped by C^+ to form C^* rather than by O^+ to form O^*. Furthermore, by finely adjusting the phase of a two-color laser pulse, the trapping of an electron to a specified ionic core can be steered. The asymmetric emission of the generated Rydberg atom in the dissociative frustrated double ionization indicates that the electron trapping is favored for CO molecules when it is exposed to the laser field pointing from C to O. The orientation-dependent electron trapping dynamics is further confirmed using a single-color elliptically polarized laser pulse, which also allows us to identify the various valence orbitals involved in the DFI process.

II. EXPERIMENTAL METHODS

As schematically illustrated in Fig. 1(a), the measurements were carried out in an ultrahigh-vacuum reaction microscope of cold target recoil ion momentum spectroscopy (COLTRIMS) [43,44], which enables us to coincidently detect the charged ions and electrons as well as the excited neutral Rydberg atoms ejected from the same molecule by using two time- and position-sensitive microchannel plate (MCP) detectors mounted on two opposite sides of the spectrometer. More details of the experimental setup can be found in our previous

*jwu@phy.ecnu.edu.cn

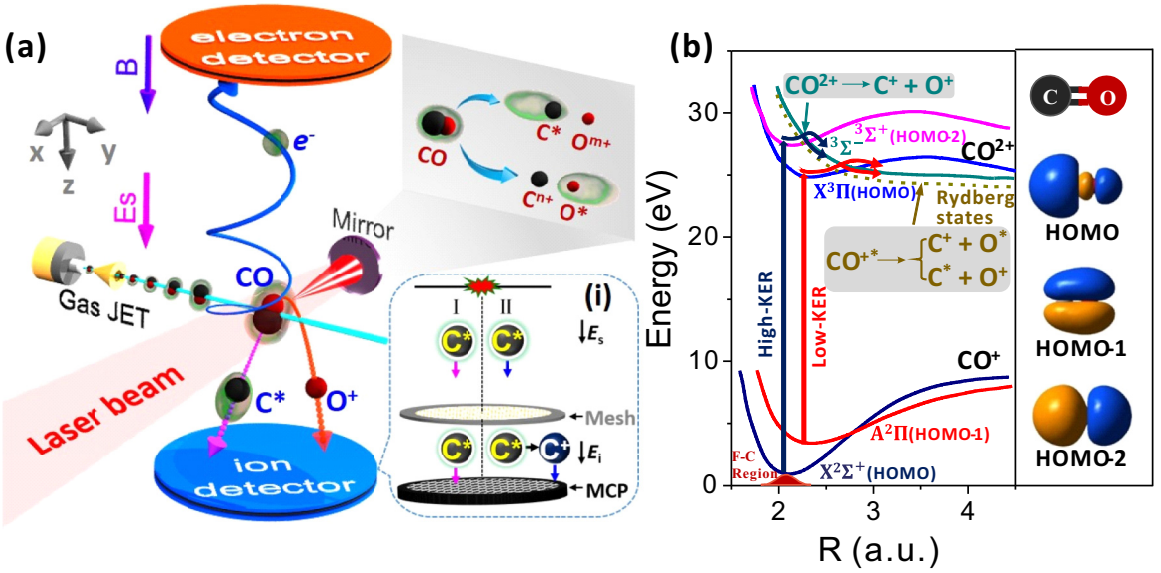

FIG. 1. (a) Schematic illustration of the experimental setup. The inset (i) shows the illustration of the spectrometer configuration of the ion side of the COLTRIMS apparatus. (b) The potential energy curves of CO^+ and CO^{2+} studied in this work. The two pathways for generating the low- and high-KER of (C^+, O^+), (C^*, O^+) and (C^+, O^*) channels are indicated by the red and navy arrows, respectively. The right panel displays the three highest occupied orbitals involved in the strong-field breaking of the CO molecule in our experiments, where the nuclei C and O lie on the left and right sides, respectively.

publications [15,28,30]. The laser-created charged ions and electrons will be guided by a homogenous static electric field ($E_s \sim 19.4\,\mathrm{V/cm}$) and a weak magnetic field ($B \sim 14.5$ G) towards the ion and electron detectors, respectively, and detected regardless of their initial ejection direction. On the other hand, the produced excited neutral Rydberg atoms can also be detected if they fly towards the ion detector and impinge on the detector with an internal potential energy larger than the work function of the MCP (a few eV) [45]. As compared to the detection of the charged particles, the detection angle of the excited neutral atoms is determined by the geometry of the spectrometer which is about 0.9π sr in our experiment [28]. The three-dimensional momenta of the detected particles were reconstructed from the measured times of flight (TOFs) and positions of the impacts during the offline analysis.

The femtosecond laser pulses (25 fs, 790 nm, 10 kHz) derived from a multipass Ti:sapphire amplifier were tightly focused onto the CO molecular beam (propagates along the y axis) using a concave silver mirror ($f = 75$ mm) inside the COLTRIMS apparatus. The CO molecules were introduced to the interaction chamber from a supersonic gas jet which generated by coexpanding a mixture of 10% CO and 90% He through a 30-μm nozzle followed by a 200-μm skimmer with a driving pressure of about 2.0 bars. In the single-color experiments, a combination of a quarter-wave plate (QWP) and a half-wave plate (HWP) was employed to adjust the laser polarization to be linear or elliptical. Both the polarization direction of the linearly polarized pulses and the major axis of the elliptically polarized pulses were rotated to be along the TOF direction of the spectrometer (the z axis). The peak intensities of the linearly and elliptically polarized laser fields in the interaction region were estimated to be $I_{\mathrm{lin}} \sim 1.1 \times 10^{15}\,\mathrm{W/cm^2}$ and $I_{\mathrm{ellip}} \sim 1.2 \times 10^{15}\,\mathrm{W/cm^2}$, respectively. To steer the electron trapping dynamics, a linearly polarized phase-controlled two-color laser pulse was generated in a collinear scheme by frequency-doubling the 25-fs near-infrared laser pulses in a 150-μm-thick β-barium borate (β-BBO) crystal, as detailed in Ref. [46]. The relative phase ϕ_{L} between the fundamental wave (FW) and second-harmonic (SH) waves of the two-color pulse can be finely varied by scanning the inset thickness of a pair of fused-silica wedges installed in the beam line. The absolute value of the ϕ_{L} is assigned by tracing the ϕ_{L}-dependent directional dissociative double ionization of CO molecules [46]. The intensities of the FW and SH components of the two-color pulse in the interaction region were estimated to be $I_{\mathrm{FW}} \sim 4.8 \times 10^{14}\,\mathrm{W/cm^2}$ and $I_{\mathrm{SH}} \sim 0.96 \times 10^{14}\,\mathrm{W/cm^2}$, respectively.

III. RESULTS AND DISSUSSIONS

When a CO molecule is exposed to an intense laser field, the molecular dissociative ionization may occur followed by the stripping of valence electrons. The cleavage of the molecular bond will generate two charged nuclei C^{n+} and O^{m+} which repel each other, forming the Coulomb explosion (CE) channels; i.e., $CO + q\hbar\omega \rightarrow C^{n+} + O^{m+}$ [denoted as (C^{n+}, O^{m+}), $n \geqslant 1$, $m \geqslant 1$]. After conclusion of the laser pulse, there is a certain probability to form the neutral Rydberg atom C^* or O^* if one of the released electrons is eventually trapped by the singly charged nuclei C^+ or O^+, leading to the DFI channels of CO; i.e., $CO + q\hbar\omega \rightarrow C^* + O^{m+}$ [denoted as (C^*, O^{m+})] and $CO + q\hbar\omega \rightarrow C^{n+} + O^*$ [denoted as (C^{n+}, O^*)]. Using the reaction microscope, the coincidence detection of all the charged and excited neutral particles ejected from the breaking molecules can be achieved.

Figure 2 displays the measured photoion-photoion coincidence (PIPICO) spectrum of the nuclear fragments produced

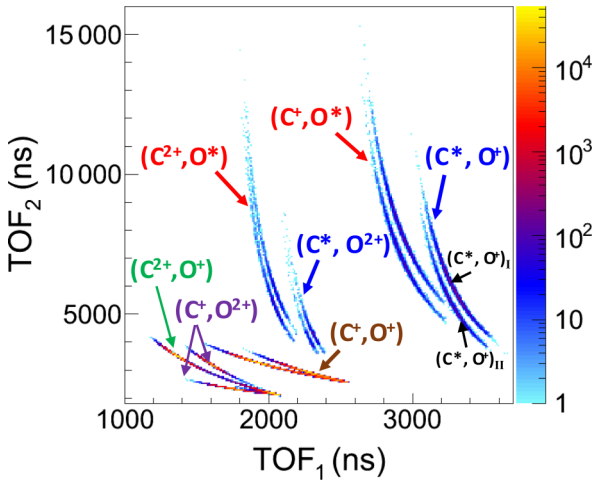

FIG. 2. Measured PIPICO spectrum of the CE and DFI channels produced from the strong-field breaking of a CO molecule using a linearly polarized 790-nm femtosecond laser pulse with an intensity of 1.1×10^{15} W/cm^2.

from the breaking of CO molecules driven by a linearly polarized 790-nm laser pulse. The excited neutral atoms (C* or O*) are generally observed in the dissociative frustrated double and triple ionization channels, accompanying the correlated charged nuclear fragments. For the ion-Rydberg nuclear fragment pairs, e.g., (C*, O$^+$) and (C$^+$, O*) pairs, due to the lack of the acceleration by the static electric fields E_s of the spectrometer, the neutral Rydberg atoms (C* or O*) fly towards the ion detector only with the momentum gained from the dissociation process. Therefore, the neutral Rydberg atoms arrive at the detector with a much larger TOF as compared to that of the charged ionic fragments (C$^+$ or O$^+$). Although the branch ratios (see Table I) of the DFI channels, e.g., (C$^+$, O*) (∼0.60%), (C*, O$^+$) (∼0.74%), (C*, O^{2+}) (∼0.10%), and (C^{2+}, O*) (∼0.19%), are rather low as compared to that of the CE channels, e.g., (C$^+$, O$^+$) (∼58.39%), (C^{2+}, O$^+$) (∼27.44%), and (C$^+$, O^{2+}) (∼12.54%), they can clearly be identified in the PIPICO spectrum as indicated by the colored arrows in Fig. 2. Interestingly, the PIPICO spectrum of each DFI channel is featured with dual PIPICO lines. For instance, as indicated by the black arrows in Fig. 2, the (C*, O$^+$) fragment pairs can be distinguished into (C*, O$^+$)$_I$ and (C*, O$^+$)$_{II}$ which are attributed to the postpulse dc-field ionization of Rydberg atoms [47–51]. As illustrated in the inset of Fig. 1, the laser-created excited Rydberg atom C* can be detected by the MCP either directly as neutral C* (with a low principal quantum number) or indirectly as charged C$^+$ following the dc-field ionization and acceleration by the static electric field E_i(∼1500 V/cm) between the mesh and MCP, which are recorded as (C*, O$^+$)$_I$ and (C*, O$^+$)$_{II}$ in the PIPICO spectrum, respectively.

By unambiguously identifying different fragmentation channels using the PIPICO spectrum, we will now turn to investigate the electron trapping dynamics in the strong-field DFI processes. Figure 3 shows the measured kinetic energy release (KER) spectra of the nuclear fragments of various dissociation channels displayed in Fig. 2. As shown in Fig. 3(a), the KER spectra of the dissociative frustrated double ionization channels (C$^+$, O*) and (C*, O$^+$) very much resemble that of the dissociative double ionization channel (C$^+$, O$^+$). In the light of previous inspections of the dissociative frustrated double ionization of molecules [26–30], the (C$^+$, O*) and (C*, O$^+$) channels should be produced in a similar approach as the (C$^+$, O$^+$) channel by trapping one of the two released electrons to the high-lying Rydberg states of the outgoing nuclear fragments. The similar KER distributions are also observed for the (C^{2+}, O$^+$) and (C^{2+}, O*) channels as shown in Fig. 3(b), and for the (C$^+$, O^{2+}) and (C*, O^{2+}) channels as shown in Fig. 3(c), respectively. It indicates that, via a comparable process as that accessed for the (C*, O$^+$) and (C$^+$, O*) channels, the (C^{2+}, O$^+$) and (C$^+$, O^{2+}) channels act as the precursors to produce the (C^{2+}, O*) and (C*, O^{2+}) fragment pairs, respectively.

For the DFI of the heteronuclear CO molecule it is interesting to inspect at which of the two nuclei (C or O) the liberated

TABLE I. The statistics data of the produced CE and DFI channels of CO molecules exposed to a linearly polarized 790-nm femtosecond laser pulse with an intensity of 1.1×10^{15} W/cm^2. The branch ratio of each channel is normalized to the total event counts of the observed dissociation channels. The electron trapping probability is estimated as the event counting ratio of the DFI channels to the total yield of the corresponding associated parent channels. The error bars of the trapping probability arise from the propagation of the statistic errors of the measured yields of each channel during the data analysis.

Dissociation channels	Events counts	Branch ratio (%)	Trapping probability (%)
(C$^+$, O$^+$)	1338535	58.39	–
(C$^+$, O*)	13832	0.60	1.03 ± 0.01 [+1 e from (C$^+$, O$^+$)]
(C*, O$^+$)	17033	0.74	1.27 ± 0.01 [+1 e from (C$^+$, O$^+$)]
(C^{2+}, O$^+$)	628891	27.44	–
(C^{2+}, O*)	4247	0.19	0.68 ± 0.01 [+1 e from (C^{2+}, O$^+$)]
(C$^+$, O^{2+})	287385	12.54	–
(C*, O^{2+})	2100	0.10	0.73 ± 0.02 [+1 e from (C$^+$, O^{2+})]
(C$^+$, O$^+$)$_{\text{low KER}}$	642365		–
(C$^+$, O*)$_{\text{low KER}}$	4978		0.78 ± 0.01 [+1 e from (C$^+$, O$^+$)$_{\text{low-KER}}$]
(C*, O$^+$)$_{\text{low KER}}$	6250		0.97 ± 0.01 [+1 e from (C$^+$, O$^+$)$_{\text{low-KER}}$]
(C$^+$, O$^+$)$_{\text{high KER}}$	696170		–
(C$^+$, O*)$_{\text{high KER}}$	8854		1.27 ± 0.01 [+1 e from (C$^+$, O$^+$)$_{\text{high KER}}$]
(C*, O$^+$)$_{\text{high KER}}$	10783		1.55 ± 0.02 [+1 e from (C$^+$, O$^+$)$_{\text{high KER}}$]

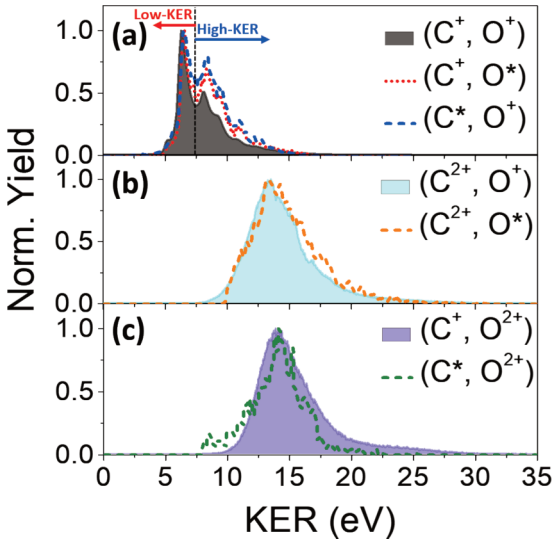

FIG. 3. The normalized KER distributions of the laser-induced CE (colored shades) and DFI (dashed lines) channels of (a) (C^+, O^+), (C^*, O^+), and (C^+, O^*), (b) (C^{2+}, O^+) and (C^{2+}, O^*), and (c) (C^+, O^{2+}) and (C^*, O^{2+}) by using a linearly polarized femtosecond laser pulse with an intensity of 1.1×10^{15} W/cm^2.

electron prefers to be eventually trapped. As listed in Table I, the electron trapping probabilities of different DFI channels are obtained by normalizing the event counts of the DFI channels to the total yield of the corresponding parent channels. To investigate the electron trapping preference of different nuclei and meanwhile exclude the effect of the charge states of the ionic core [35], we here concentrate on the (C^+, O^*) and (C^*, O^+) channels as an example since they are originated from the same precursor, i.e., the charge symmetric (C^+, O^+) channel. The corresponding probability for the electron trapping to nucleus C and O in these two channels are calculated by using the formulas of $P_{(C^*)} = Y_{(C^*,O^+)}/Y_{(C^+,O^+)}$, and $P_{(O^*)} = Y_{(C^+,O^*)}/Y_{(C^+,O^+)}$, respectively. Interestingly, as listed in Table I, the probability for the electron trapping by nucleus C ($\sim 1.27 \pm 0.01\%$) to form the (C^*, O^+) channel is higher than that being captured by nucleus O ($\sim 1.03 \pm 0.01\%$) in producing the (C^+, O^*) channel, which is in contradiction with the fact that the electronegativity of C^+ is smaller than that of O^+ [52]. The error bars of the trapping probability represent the propagation error that transferred from the statistic error of the measured yield to the calculated trapping probability according to the equation

$$P_{(\text{error})} = P_{(\text{trapping probability})}\sqrt{[\delta Y_{(\text{DFI channel})}/Y_{(\text{DFI channel})}]^2 + [\delta Y_{(\text{precursor channel})}/Y_{(\text{precursor channel})}]^2}.$$

Here the $P_{(\text{trapping probability})}$ and $P_{(\text{error})}$ are the calculated electron trapping probabilities and the corresponding errors; $Y_{(\text{DFI channel})}$ and $Y_{(\text{precursor channel})}$, are the yields of the involved DFI channel and its precursor channel, and the corresponding statistic yield errors of these two channels are denoted as $\delta Y_{(\text{DFI channel})}$ and $\delta Y_{(\text{precursor channel})}$, respectively. We note that the detection efficiencies of the MCP for C^* and O^* are similar and thus have a negligible influence on the here-observed preference of electron trapping, which is further confirmed by only considering electron trapping events for the dc-ionized Rydberg fragments [53]. In the following, we will show that the preference of the electron trapping to C rather than O is related to the orientation-dependent ionization of CO molecules.

Driven by a phase-controlled linearly polarized two-color laser pulse, the asymmetric emission of a produced Rydberg atom C^* or O^* in the DFI of CO can be finely steered. Figures 4(a) and 4(b) display the ϕ_L-dependent yield of the (C^*, O^+) and (C^+, O^*) pairs as a function of the KER of the nuclear fragments, respectively, where opposite phase-dependent oscillations are observed. Note that the yield modulations of the (C^*, O^+) and (C^+, O^*) pairs in Figs. 4(a) and 4(b) stand for the directional ejection of C^* and O^*, respectively, since only the Rydberg atoms flying towards the ion detector could be measured in our experimental configuration. To quantify the directional emission of C^* and O^*, we define the asymmetry parameter as $A(\phi_L) = [N(\phi_L) - N(\phi_L + \pi)]/[N(\phi_L) + N(\phi_L + \pi)]$, where $N(\phi_L)$ and $N(\phi_L + \pi)$ are the yields of the DFI fragment pairs at the laser phase of ϕ_L and $\phi_L + \pi$, respectively. As displayed in Figs. 4(c) and 4(d), the corresponding ϕ_L-dependent asymmetries of C^* and O^* are featured with oscillating amplitudes of about 20%. The positive or negative values of $A(\phi_L)$ stand for the favorable emission of the Rydberg atoms towards $(+z)$ or opposite $(-z)$ to the ion detector, respectively.

As schematically illustrated in Figs. 4(c) and 4(d), the changing of phase ϕ_L alters the orientation of the field maximum of the linearly polarized two-color laser pulse along the TOF axis (z axis) of our experimental geometry, which points to $+z$ and $-z$ for $\phi_L = 0$ and π, respectively. Interestingly, the ϕ_L-dependent asymmetries of C^* and O^* clearly indicate that the Rydberg atoms are favored to be formed when the laser field points from C to O in the CO molecule. Governed by the profiles of the ionizing orbitals, it has been demonstrated that the CO molecule is favored to be ionized by the laser field pointing from C towards O [37–40]. The higher ionization rate when the laser field points from C to O will produce more parent ions as the precursors and increase the electron trapping probability to form the Rydberg atoms. Moreover, it is shown that the laser-created O^* mostly emits along the direction of the maximum of the asymmetric optical fields and the C^* has the opposite emission direction. For instance, at $\phi_L = 0$ where the field maximum of the laser field points to $+z$, the O^* prefers to emit to the $+z$ direction as shown in Fig. 4(d), while the C^* is favored to emit to the $-z$ direction as displayed in Fig. 4(c). The observed asymmetric emission of the produced Rydberg atoms is ascribed to the ϕ_L-dependent asymmetric electron trapping dynamics, which is also responsible for different electron trapping probability to the C and O atoms. In general, the electrons tunneled out around the peak of the laser field will obtain sufficiently small drift momentum and there

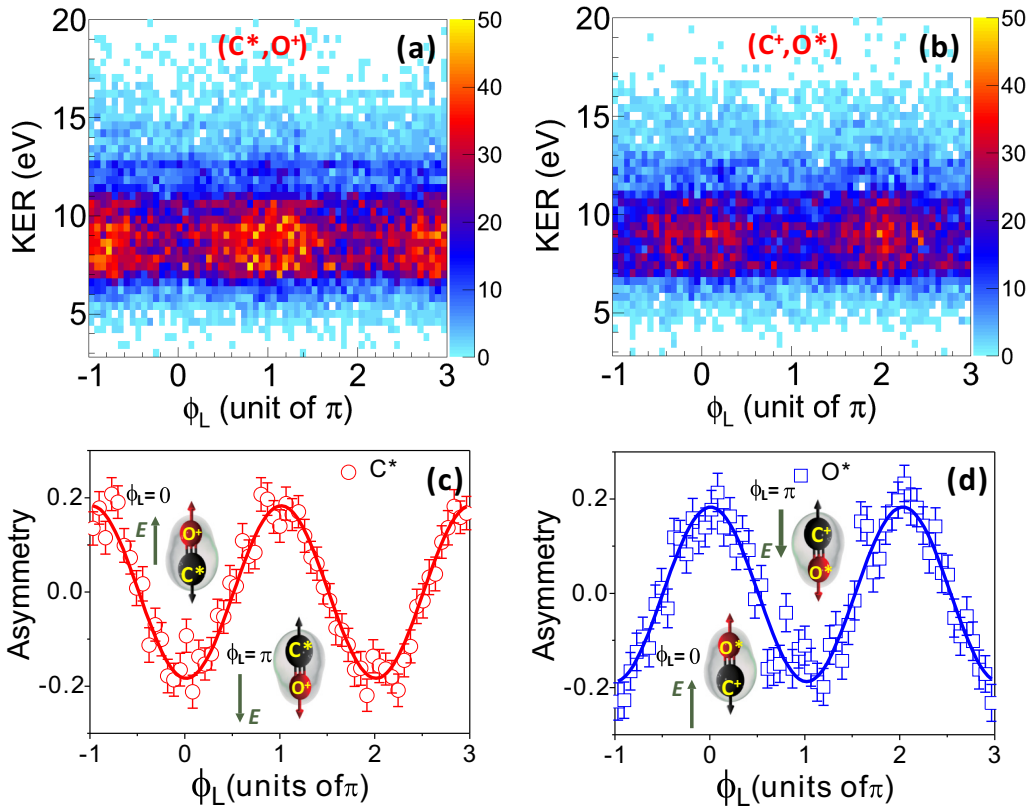

FIG. 4. Measured KER-dependent yields of the (a) (C^*, O^+) and (b) (C^+, O^*) pairs as a function of relative phase ϕ_L of a linearly polarized two-color laser pulse. The corresponding calculated ϕ_L-dependent asymmetries of the directional emission of (a) C^* of the (C^*, O^+) channel and (b) O^* of the (C^+, O^*) channel. The solid curves are the numerical fit of the experimental data.

is a large probability that they can be ultimately recaptured by the outgoing charged nuclei. The prior findings show that the electron emitting before the peak of the laser field is more likely to be recaptured as compared to those emitting after the laser peak [54,55]. The electrons released before the positive peak of the optical field will finally acquire a drift momentum in the $-z$ direction and these electrons are prone to being recaptured by the parallel-propagating nucleus C rather than the antiparallel-propagating nucleus O.

The orientation-dependent directional dissociative frustrated double ionization of CO molecules also generally occurs in the single-color laser pulse as we confirmed in the following using elliptically polarized femtosecond laser pulses. Although the absolute electron trapping probability decreases for the elliptically polarized laser pulse, the relative probabilities of the electron to be recaptured to nucleus C or O is consistent with that in a linearly polarized pulse. In the elliptically polarized pulses, the electron is mainly freed when the laser field points along the major axis and receives a final momentum along the minor axis owing to the angular streaking of the rotating electric field [30,40,56]. Hence, the direction of the laser field vector at the instant of ionization is encoded in the momentum direction of the released electron along the minor polarization axis (y axis). As sketched in the inset of Fig. 5(a), for the here-employed anticlockwise rotating elliptical field (ellipticity $\varepsilon\sim0.18$) with major axis along the z direction and minor axis along the y direction, the freed electrons with final momentum of positive ($py_e > 0$) or negative ($py_e < 0$) along the y axis are liberated by the instantaneous laser field pointing to the $+z$ or $-z$ directions, respectively. Therefore, any possible laser field-dependent asymmetry in the breaking of an oriented CO molecule along the z axis will be mapped in the asymmetry of the electron momentum distribution along the y axis. For instance, the recognized feature of the orientation-dependent asymmetric ionization rate of CO is encoded in the asymmetric py_e distributions. Figure 5(a) displays the momentum distributions of two freed electrons on top of each other for the (C^+, O^+) channel. The distinct asymmetric distribution of py_e can be observed if the ejection direction of the C^+ ion is gated to $+z(pz_{C+} > 0)$ or $-z(pz_{C+} < 0)$, corresponding to the initial orientation of CO with the C atom pointing to $+z$ or $-z$, respectively. As shown in Fig. 5(a), the enhancement in the yield at $py_e > 0$ (or $py_e < 0$) for $pz_{C+} < 0(pz_{C+} > 0)$ suggests a higher dissociative ionization rate when the laser field is pointing to $+z$ (or $-z$), which is opposite to the orientation direction of atom C. It is in accordance with the conclusions drawn in early studies [37–40] that the double ionization of CO is more likely to occur when it is exposed to the laser field pointing from C to O.

The asymmetric momentum distribution of the ionization-created freed electron also allows us to reveal the directional emission of the Rydberg atoms in the DFI of CO. For the dissociative frustrated double ionization of CO, among the two released electrons only one electron is freed while the other is trapped to the nuclei. Figures 5(b) and 5(c)

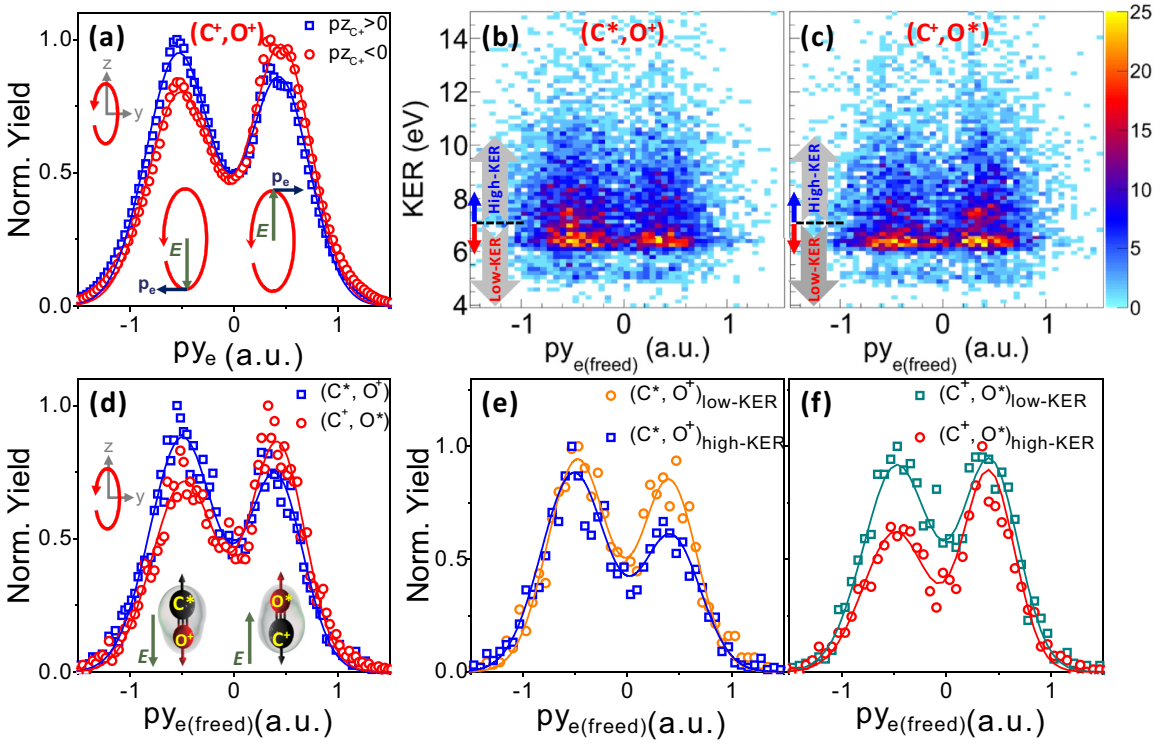

FIG. 5. (a) The measured electron momentum distributions of the (C^+, O^+) channel along the minor polarization axis (y axis, py_e) of the elliptically polarized pulse. The blue and red distributions corresponding to the applied condition of the C^+ emitting to the positive ($pz_{C+} > 0$) or negative ($pz_{C+} < 0$) direction of the z axis, respectively. (b), (c) The KER-dependent momentum distributions ($py_{e(\text{freed})}$) of the freed electron measured from the (b) (C^*, O^+) and (c) (C^+, O^*) channels. The corresponding $py_{e(\text{freed})}$ distributions integrated over different KER ranges are plotted in (d)–(f). The solid curves in (a) and (d)–(f) are the numerical fit of the distributions which act as guides to the eye. The units of a.u. is the abbreviation of atomic units.

display the KER-dependent momentum distributions of the freed electron $py_{e(\text{freed})}$ measured from the (C^*, O^+) and (C^+, O^*) channels, respectively. The $py_{e(\text{freed})}$ distributions of both channels are featured with two peaks centered at $py_{e(\text{freed})} = \pm 0.5$ a.u., which very much resemble the py_e distribution of the (C^+, O^+) channel. As shown in Fig. 5(d), the KER integrated $py_{e(\text{freed})}$ distributions of the (C^*, O^+) and (C^+, O^*) channels show distinct asymmetric distributions. Note that the initial orientation of CO in these two channels is preassigned by the gates of $pz_{C^*} > 0$ for the (C^*, O^+) channel and $pz_{O^*} > 0$ for the (C^+, O^*), channel which are determined by our experimental configuration. Similar to the (C^+, O^+) channel, the higher side peak at $py_{e(\text{freed})} > 0$ for the (C^+, O^*) channel or $py_{e(\text{freed})} < 0$ for the (C^*, O^+) channel indicates that the DFI rate is higher when the laser field points to $+z$ or $-z$, correspondingly. Since the measured freed electron is correlated to the nuclear fragments, the asymmetric $py_{e(\text{freed})}$ distribution shown in Fig. 5(d) also suggests that the Rydberg atom O^* and C^* are favored to be produced when the laser field is pointing from C to O, which is in agreement with our above observations in the measurements using the phase-controlled two-color pulses.

More interestingly, as marked by the arrows in Figs. 5(b) and 5(c), the $py_{e(\text{freed})}$ distributions of both the (C^*, O^+) and (C^+, O^*) channels are featured with different asymmetries for the high- and low-KER regions separated by 0.7 eV. This KER dependence of the asymmetries can be noticed more clearly by integrating over the low- (KER $<$ 0.7 eV) and high-KER (KER $>$ 0.7 eV) regions, as shown in Figs. 5(e) and 5(f). For both the (C^*, O^+) and (C^+, O^*) channels, the $py_{e(\text{freed})}$ corresponding to the high-KER region shows a larger asymmetry than that of the low-KER region. The KER-dependent distinct asymmetries also exhibit in the (C^+, O^+) channel (data not shown). Generally, multiple orbitals and electronic states will be involved in the strong-field breaking of CO molecules [39–42]. As we will discuss below, the distinct asymmetries of the low- and high-KER regions correlate with the releasing of electrons from different orbitals.

As illustrated in Fig. 1(b), the stepwise pathways involving different orbitals are identified to produce the double ionization channel of (C^+, O^+) and the associated DFI channel of (C^*, O^+) and (C^+, O^*). Starting from the population of the ionic bound states $X\,^2\Sigma^+$ or $A\,^2\Pi$ of CO^+ by removing of the first electron from the highest occupied molecular orbital (HOMO) or HOMO-1, the subsequent removal of the second electron from HOMO-2 or HOMO leads to the population of the bound states $^3\Sigma^+$ or $X^3\Pi$ of CO^{2+}, respectively, which afterwards dissociates through the crossing repulsive potential curve (e.g., $^3\Sigma^-$), forming the Coulomb exploded double ionization channel of (C^+, O^+). There is also a certain probability that the high-lying Rydberg states of CO^+ (i.e., the CO^{+*} states) which are very close to the dissociating CO^{2+} state can be populated during the crossing transition, leading to the eventual dissociation into the (C^*, O^+) or (C^+, O^*) channel. The dissociation followed by the vertical transition of $X\,^2\Sigma^+ - {}^3\Sigma^+$ will lead -to a higher KER as compared to that

by the $A\,^2\Pi - X\,^3\Pi$ transition because the former transition occurs at the shorter equilibrium internuclear distance. It thus suggests that the low- and high-KER peaks in the (C^*, O^+) and (C^+, O^*) channels are contributed by the releasing of electrons from the orbitals of (HOMO, HOMO-1) and (HOMO, HOMO-2), respectively, but one of the two liberated electrons is eventually trapped by the outgoing ionic fragments. As shown in Fig. 1(b), these three orbitals are featured with different profiles and the electron densities mainly locate on the C side for the HOMO and HOMO-2. Therefore, a larger asymmetry in the ionization rate is expected when the electron is released from these two orbitals. The combined contribution of the asymmetry given by the HOMO and HOMO-2 thus leads to larger asymmetries in the high-KER region than that of the low-KER region where the asymmetries along the laser polarization are mainly contributed from the releasing electron from the HOMO. Moreover, the observed KER-dependent asymmetries of the $py_{e(\text{freed})}$ also suggests a KER-dependent electron trapping probability in producing the Rydberg atom C^* or O^*. This can be confirmed by examining the KER distributions and electron trapping probabilities measured in the linearly polarized single-color laser fields. As shown in Fig. 3(a), the KER distributions of the (C^+, O^+), (C^*, O^+), and (C^+, O^*) channels are also separated into low- and high-KER regions. As compared to the low-KER region, noticeable enhanced yield at high KER of the (C^*, O^+) and (C^+, O^*) channels with respect to that of the (C^+, O^+) channel can be observed. The correspondingly estimated electron trapping probabilities for the low- and high-KER regions are listed in Table I. The electron trapping probability for the high-KER region of the (C^*, O^+) ($\sim 1.55 \pm 0.02\%$) or (C^+, O^*) ($\sim 1.27 \pm 0.01\%$) channel is much higher than that of the low-KER region, which is $\sim 0.97 \pm 0.01\%$ and $\sim 0.78 \pm 0.01\%$ for the (C^*, O^+) and (C^+, O^*) channel, respectively.

IV. CONCLUSION

In conclusion, the formation of neutral Rydberg atoms C^* or O^* in strong-field DFI of CO molecules was experimentally investigated. The neutral Rydberg and charged nuclear fragments as well as the freed electron ejected from a breaking molecule were measured in coincidence with a reaction microscope, which allows us to trace the electron trapping probabilities in different DFI channels. It was found that the electron prefers to be trapped by C^+ rather than O^+ to form the Rydberg atoms. Furthermore, the asymmetric emission of the Rydberg atoms can be steered by using a phase-controlled two-color laser pulse, which is confirmed to generally occur in a single-color elliptically polarized laser pulse. Our results show that the Rydberg atom is favored to be formed when it is exposed to a laser field pointing from C to O.

ACKNOWLEDGMENTS

This work is supported by the National Key R&D Program of China (Grant No. 2018YFA0306303), the National Natural Science Fund (Grants No. 11834004, No. 61690224, No. 11761141004, and No. 11704124), the 111 project of China (Grant No. B12024), Projects from Shanghai Science and Technology Commission (Grant No. 19JC1412200), and the Shanghai Sailing Program (Grant No. 17YF1404000). W.Z. acknowledges the support from the Outstanding Doctoral Dissertation Cultivation Plan of Action (Grant No. YB2016036) and the Future Scientist Cultivation Program of ECNU.

[1] P. Agostini, F. Fabre, G. Mainfray, G. Petite, and N. K. Rahman, Phys. Rev. Lett. **42**, 1127 (1979).
[2] R. R. Freeman, P. H. Bucksbaum, H. Milchberg, S. Darack, D. Schumacher, and M. E. Geusic, Phys. Rev. Lett. **59**, 1092 (1987).
[3] D. N. Fittinghoff, P. R. Bolton, B. Chang, and K. C. Kulander, Phys. Rev. Lett. **69**, 2642 (1992).
[4] B. Walker, B. Sheehy, L. F. DiMauro, P. Agostini, K. J. Schafer, and K. C. Kulander, Phys. Rev. Lett. **73**, 1227 (1994).
[5] M. Meckel, D. Comtois, D. Zeidler, A. Staudte, D. Pavicic, H. C. Bandulet, H. Pepin, J. C. Kieffer, R. Dorner, D. M. Villeneuve, and P. B. Corkum, Science **320**, 1478 (2008).
[6] C. I. Blaga, J. Xu, A. D. DiChiara, E. Sistrunk, K. Zhang, P. Agostini, T. A. Miller, L. F. DiMauro, and C. D. Lin, Nature (London) **483**, 194 (2012).
[7] M. G. Pullen, B. Wolter, A.-T. Le, M. Baudisch, M. Hemmer, A. Senftleben, C. D. Schröter, J. Ullrich, R. Moshammer, C. D. Lin, and J. Biegert, Nat. Commun. **6**, 7262 (2015).
[8] M. Ferray, A. L'Huillier, X. F. Li, L. A. Lomprk, G. Mainfray, and C. Manus, J. Phys. B **21**, L31 (1988).
[9] P. B. Corkum, Phys. Rev. Lett. **71**, 1994 (1993).
[10] M. P. de Boer and H. G. Muller, Phys. Rev. Lett. **68**, 2747 (1992).
[11] R. R. Jones, D. W. Schumacher, and P. H. Bucksbaum, Phys. Rev. A **47**, R49 (1993).
[12] U. Eichmann, A. Saenz, S. Eilzer, T. Nubbemeyer, and W. Sandner, Phys. Rev. Lett. **110**, 203002 (2013).
[13] G. N. Gibson, L. Fang, and B. Moser, Phys. Rev. A **74**, 041401(R) (2006).
[14] Q. Li, X. M. Tong, T. Morishita, H. Wei, and C. D. Lin, Phys. Rev. A **89**, 023421 (2014).
[15] W. Zhang, X. Gong, H. Li, P. Lu, F. Sun, Q. Ji, K. Lin, J. Ma, H. Li, and J. Qiang *et al.*, Nat. Commun. **10**, 757 (2019).
[16] J. Ma, W. Zhang, K. Lin, Q. Ji, H. Li, F. Sun, J. Qiang, F. Chen, J. Tong, P. Lu, H. Li, X. Gong, and J. Wu, Phys. Rev. A **100**, 063413 (2019).
[17] B. B. Wang, X. F. Li, P. M. Fu, J. Chen, and J. Liu, Chin. Phys. Lett. **23**, 2729 (2006).
[18] T. Nubbemeyer, K. Gorling, A. Saenz, U. Eichmann, and W. Sandner, Phys. Rev. Lett. **101**, 233001 (2008).
[19] S. Larimian, C. Lemell, V. Stummer, J. W. Geng, S. Roither, D. Kartashov, L. Zhang, M. X. Wang, Q. Gong, L. Y. Peng, S. Yoshida, J. Burgdörfer, A. Baltuška, M. Kitzler, and X. Xie, Phys. Rev. A **96**, 021403(R) (2017).
[20] U. Eichmann, T. Nubbemeyer, H. Rottke, and W. Sandner, Nature (London) **461**, 1261 (2009).

[21] S. D. Hogan, C. Seiler, and F. Merkt, Phys. Rev. Lett. **103**, 123001 (2009).

[22] W. H. Xiong, J. W. Geng, J. Y. Tang, L. Y. Peng, and Q. Gong, Phys. Rev. Lett. **112**, 233001 (2014).

[23] H. Liu, Y. Liu, L. Fu, G. Xin, D. Ye, J. Liu, X. T. He, Y. Yang, X. Liu, Y. Deng, C. Wu, and Q. Gong, Phys. Rev. Lett. **109**, 093001 (2012).

[24] M. Fushitani, C. N. Liu, A. Matsuda, T. Endo, Y. Toida, M. Nagasono, T. Togashi, M. Yabashi, T. Ishikawa, Y. Hikosaka, T. Morishita, and A. Hishikawa, Nat. Photonics **10**, 102 (2016).

[25] H. Yun, J. H. Mun, S. I. Hwang, S. B. Park, I. A. Ivanov, C. H. Nam, and K. T. Kim, Nat. Photonics **12**, 620 (2018).

[26] B. Manschwetus, T. Nubbemeyer, K. Gorling, G. Steinmeyer, U. Eichmann, H. Rottke, and W. Sandner, Phys. Rev. Lett. **102**, 113002 (2009).

[27] A. Emmanouilidou, C. Lazarou, A. Staudte, and U. Eichmann, Phys. Rev. A **85**, 011402(R) (2012).

[28] W. Zhang, Z. Yu, X. Gong, J. Wang, P. Lu, H. Li, Q. Song, Q. Ji, K. Lin, J. Ma, H. X. Li, F. Sun, J. Qiang, H. Zeng, F. He, and J. Wu, Phys. Rev. Lett. **119**, 253202 (2017).

[29] J. McKenna, S. Zeng, J. J. Hua, A. M. Sayler, M. Zohrabi, N. G. Johnson, B. Gaire, K. D. Carnes, B. D. Esry, and I. Ben-Itzhak, Phys. Rev. A **84**, 043425 (2011).

[30] W. Zhang, H. Li, X. Gong, P. Lu, Q. Song, Q. Ji, K. Lin, J. Ma, H. Li, F. Sun, J. Qiang, H. Zeng, and J. Wu, Phys. Rev. A **98**, 013419 (2018).

[31] T. Nubbemeyer, U. Eichmann, and W. Sandner, J. Phys. B **42**, 134010 (2009).

[32] J. McKenna, A. M. Sayler, B. Gaire, N. G. Kling, B. D. Esry, K. D. Carnes, and I. Ben-Itzhak, New J. Phys. **14**, 103029 (2012).

[33] B. Ulrich, A. Vredenborg, A. Malakzadeh, M. Meckel, K. Cole, M. Smolarski, Z. Chang, T. Jahnke, and R. Dörner, Phys. Rev. A **82**, 013412 (2010).

[34] B. Manschwetus, H. Rottke, G. Steinmeyer, L. Foucar, A. Czasch, H. Schmidt-Böcking, and W. Sandner, Phys. Rev. A **82**, 013413 (2010).

[35] J. Wu, A. Vredenborg, B. Ulrich, L. Ph. H. Schmidt, M. Meckel, S. Voss, H. Sann, H. Kim, T. Jahnke, and R. Dorner, Phys. Rev. Lett. **107**, 043003 (2011).

[36] X. Xie, C. Wu, H. Liu, M. Li, Y. Deng, Y. Liu, Q. Gong, and C. Wu, Phys. Rev. A **88**, 065401 (2013).

[37] H. Ohmura, N. Saito, and T. Morishita, Phys. Rev. A **83**, 063407 (2011).

[38] H. Li, D. Ray, S. De, I. Znakovskaya, W. Cao, G. Laurent, Z. Wang, M. F. Kling, A. T. Le, and C. L. Cocke, Phys. Rev. A **84**, 043429 (2011).

[39] I. Znakovskaya, P. von den Hoff, S. Zherebtsov, A. Wirth, O. Herrwerth, M. J. J. Vrakking, R. de Vivie-Riedle, and M. F. Kling, Phys. Rev. Lett. **103**, 103002 (2009).

[40] J. Wu, L. Ph. H. Schmidt, M. Kunitski, M. Meckel, S. Voss, H. Sann, H. Kim, T. Jahnke, A. Czasch, and R. Dörner, Phys. Rev. Lett. **108**, 183001 (2012).

[41] W. Zhang, Z. Li, P. Lu, X. Gong, Q. Song, Q. Ji, K. Lin, J. Ma, F. He, H. Zeng, and J. Wu, Phys. Rev. Lett. **117**, 103002 (2016).

[42] Q. Song, Z. Li, H. Li, P. Lu, X. Gong, Q. Ji, K. Lin, W. Zhang, J. Ma, H. Zeng, F. He, and J. Wu, Opt. Express **25**, 2221 (2017).

[43] R. Dörner, V. Mergel, O. Jagutzki, L. Spielberger, J. Ullrich, R. Moshammer, and H. Schmidt-Böcking, Phys. Rep. **330**, 95 (2000).

[44] J. Ullrich, R. Moshammer, A. Dorn, R. Dörner, L. P. H. Schmidt, and H. Schmidt-Böcking, Rep. Prog. Phys. **66**, 1463 (2003).

[45] B. Berry, M. Zohrabi, D. Hayes, U. Ablikim, B. Jochim, T. Severt, K. D. Carnes, and I. Ben-Itzhak, Rev. Sci. Instrum. **86**, 046103 (2015).

[46] J. Wu, A. Vredenborg, L. Ph. H. Schmidt, T. Jahnke, A. Czasch, and R. Dörner, Phys. Rev. A **87**, 023406 (2013).

[47] T. F. Gallagher, *Rydberg Atoms* (Cambridge University Press, Cambridge, UK, 2005), Vol. 6.

[48] H. Zimmermann, J. Buller, S. Eilzer, and U. Eichmann, Phys. Rev. Lett. **114**, 123003 (2015).

[49] E. Diesen, U. Saalmann, M. Richter, M. Kunitski, R. Dörner, and J. M. Rost, Phys. Rev. Lett. **116**, 143006 (2016).

[50] H. Lv, W. Zuo, L. Zhao, H. Xu, M. Jin, D. Ding, S. Hu, and J. Chen, Phys. Rev. A **93**, 033415 (2016).

[51] S. Larimian, S. Erattupuzha, C. Lemell, S. Yoshida, S. Nagele, R. Maurer, A. Baltuška, J. Burgdörfer, M. Kitzler, and X. Xie, Phys. Rev. A **94**, 033401 (2016).

[52] H. O. Pritchard and H. A. Skinner, Chem. Rev. **55**, 745 (1955).

[53] F. Sun, W. Zhang, P. Lu, Q. Song, K. Lin, Q. Ji, J. Ma, H. Li, J. Qiang, X. Gong, H. Li, and J. Wu, J. Phys. B **53**, 035601 (2020).

[54] N. I. Shvetsov-Shilovski, S. P. Goreslavskia, S. V. Popruzhenkoa, and W. Becker, Laser Phys. **19**, 1550 (2009).

[55] A. S. Landsman, A. N. Pfeiffer, C. Hofmann, M. Smolarski, C. Cirelli, and U. Keller, New J. Phys. **15**, 013001 (2013).

[56] J. Wu, M. Meckel, L. Ph. H. Schmidt, M. Kunitski, S. Voss, H. Sann, H. Kim, T. Jahnke, A. Czasch, and R. Dörner, Nat. Commun. **3**, 1113 (2012).